analytica

MDPI

Article

A Novel ppb-Level Sensitive and Highly Selective Europium-Based Diketone Luminescent Sensor for the Quantitative Detection of Aluminum Ions in Water Samples

Nawagamu A. K. Rajitha Perera †, Sindhu K. Shankar, Cynthia M. Archambault, Vladimir N. Nesterov, Sreekar B. Marpu, Hao Yan * and Mohammad A. Omary *

Department of Chemistry, University of North Texas, Denton, TX 76203, USA; rajithaperera@my.unt.edu (N.A.K.R.P.); sindhukonanurshankar@my.unt.edu (S.K.S.); vladimir.nesterov@unt.edu (V.N.N.); sreekarbabu.marpu@unt.edu (S.B.M.)

* Correspondence: hao.yan@unt.edu (H.Y.); omary@unt.edu (M.A.O.)

† First author and the main investigator.

Abstract: A novel Eu(tta)$_3$([4,4′-(t-bu)$_2$-2,2′-bpy)] complex (tta-thenoyltrifluoroacetone), a ratiometric luminescent-based optical sensor for the quantitative determination of aluminum ion, is synthesized and characterized using XRD and ^{1}H NMR. The XRD data reveal the slightly distorted octahedral structure. The complex displays a bright red emission at 613 nm in methanol which is characteristic of europium (III) complexes. Upon the addition of Al^{3+} ions, the red emission disappears, and a new blue emission at 398 nm emerges, manifesting the ratiometric nature of the complex. The turn-off of the red emission and turn-on of the blue emission are attributed to Eu-Al transmetalation, as supported by Raman data that show the emergence of Al-O vibrations at 418, 495, and 608 cm^{-1} concomitant with the disappearance of Eu-O and Eu-N bond vibrations. Most aluminum sensors are known to suffer from interferences from other metals including Cu^{2+}, Co^{2+}, and Cd^{2+}. However, the sensor reported here is tested for 11 common cations and shows no interference on sensitivity. To the best of our knowledge, this is the first known Eu-based luminescence sensor that successfully exhibited the ability to detect aluminum ions in ppb levels in aqueous environments. The calculated Al^{3+} binding constant is $2.496 \times 10^3 \pm 172$. The complex shows a linear relationship in the range of 0–47.6 ppb (1.76×10^{-6} M) Al^{3+} and the limit of detection (LOD) is 4.79 ppb (1.77×10^{-7} M) in MeOH. ICP-OES is used for validation of the sensor complex in water and then it was used for quantitative detection of Al^{3+} ions in water as a real-life application. The complex can accurately detect Al^{3+} ions in the range of 4.97–24.9 ppb (1.84×10^{-7} M–9.2×10^{-7} M) with an LOD of 8.11 ppb (2.99×10^{-7} M). Considering that the aluminum ion serves no recognized function within the human body, its accumulation can lead to severe neurological disorders, including Parkinson's and Alzheimer's diseases. With the LOD value significantly lower than the WHO-recommended maximum permissible level of 200 ppb for aluminum in drinking water, even without high-power laser-aided signal enhancement, the sensor shows promise for detecting trace amounts of aluminum contamination in water. Therefore, it can significantly aid in the monitoring of even the smallest aluminum ion contamination in drinking water, industrial effluents, and natural water bodies.

Keywords: photoluminescence; emission; sensor; calibration; aluminum; ppb; Europium

Citation: Perera, N.A.K.R.; Shankar, S.K.; Archambault, C.M.; Nesterov, V.N.; Marpu, S.B.; Yan, H.; Omary, M.A. A Novel ppb-Level Sensitive and Highly Selective Europium-Based Diketone Luminescent Sensor for the Quantitative Detection of Aluminum Ions in Water Samples. *Analytica* **2023**, *4*, 432–446. https://doi.org/10.3390/analytica4040031

Academic Editor: Marcello Locatelli

Received: 28 September 2023
Revised: 2 November 2023
Accepted: 2 November 2023
Published: 6 November 2023

1. Introduction

In recent years, there has been growing interest among researchers in the development of highly selective and sensitive luminescent optical sensors, due to their potential use in a variety of real-life applications, including clinical, medical, environmental, and living systems [1–7]. These sensors are notably appealing due to their capability to discern various metal ions, encompassing a spectrum of transition and hazardous metal ions,

rendering them highly valuable for a wide array of practical applications [1–7]. Among these ions, aluminum is the most abundant in the Earth's crust and is extensively used in day-to-day life [8,9]. However, aluminum is not an essential element for the human body and can bind with proteins that have the capacity to carry iron [10]. The main sources of aluminum uptake in the human body are food additives, occupational ducts, pharmaceuticals, and cooking equipment [8,9]. Excessive intake of aluminum can lead to adverse effects [10], including central nervous system damage that can result in Parkinson's disease and Alzheimer's disease, due to unregulated Al^{3+} ions in the human body [7]. Additionally, excessive intake of aluminum ions can damage the kidneys [11] and work as a competitive inhibitor for essential ions, including Fe^{2+}, Mg^{2+}, and Ca^{2+} [12]. As a result, the development of highly selective and sensitive luminescent optical sensors for the detection of aluminum ions has become an important area of research, with potential implications for a variety of practical applications.

Various analytical techniques, such as atomic absorption spectroscopy, inductively coupled plasma atomic emission spectroscopy, and inductively coupled plasma mass spectroscopy, have traditionally been employed as the primary detection methods for sensing Al^{3+} ions. However, these methods are expensive, complicated, and require pre-treatment steps and specialized instruments [13,14]. Luminescence spectroscopy, on the other hand, is a more favorable method due to its operational simplicity, instant response, high selectivity, and non-destructive nature for living cells [13,14]. Nevertheless, compared to other heavy-metal ions, the detection of Al^{3+} ions presents unique challenges due to their poor coordination ability and lack of spectroscopic character [7]. Most of the previously reported fluorophores for detecting aluminum ions have suffered from complex synthesis procedures, insolubility in polar solvents, shorter luminescent lifetimes, narrow energy gaps, and interferences from other metals, such as Cu^{2+}, Co^{2+}, and Cd^{2+} [7,14]. Therefore, developing a reliable and practical luminescence-based sensing method for detecting Al^{3+} ions is an ongoing challenge in the field of analytical chemistry.

The detection of aluminum content in water is of great importance. In 1989, the World Health Organization declared aluminum ions as a food pollutant and set a limit of 200 μg L^{-1} (200 ppb, 7.41 μM) for drinking water [6,15]. High concentrations of aluminum in the atmosphere, soil, and water can have adverse effects on the growth of plants and animals [13]. Improperly treated water can also pose serious threats to patients with chronic renal disease [12]. Nearly 40% of acidified soil worldwide is the result of water-soluble aluminum ion leaching [16]. Aluminum carbonate, aluminum oxide, and aluminum nitride are the primary components of aluminum production waste (APW), which is often disposed of in landfills. Despite remaining dormant for years, landfilled APW can react exothermically with water-soluble leaching from the APW matrix, resulting in toxic soil [16,17]. All of this information underscores the critical need to detect Al^{3+} ions selectively and quantitatively in water.

Luminescence-based aluminum probes have been developed using various approaches. Most of the sensor molecules are metal-free organic molecules that recognize and re-arrange the molecule in the presence of aluminum ions (guest) via covalent interactions [6–9,11,12,15]. Some probes utilize gold nanoparticles for aluminum ion detection [10,18]. Metal-based complexes for aluminum ion detection are not widely reported in the literature, as metalated complexes may undergo trans-metalation. However, such complexes can exhibit not only effective aluminum sensing properties but also function as aluminum ion removers [19].

Lanthanide complexes have found utility not only in the detection of metal ions, such as Al^{3+}, K^{+}, and Zn^{2+}, but also in anion and gas [10,20–23]. However, due to the Laporte-forbidden nature of f-f transitions [24], lanthanide complexes exhibit weak luminescence, characterized by low extinction coefficients typically in the range of 0.5–3 L mol^{-1} cm^{-1} [24]. Consequently, the luminescence of lanthanide cations necessitates the use of ligand sensitization [24]. Sensitizer ligands typically consist of aromatic or unsaturated organic molecules with anionic or dipolar properties to facilitate effective binding to the +3 metal center [25].

For this process to be successful, the ligand must meet a crucial prerequisite: the energy gap between the ligand's triplet state and the lanthanide's emitting excited state (e.g., $^5D_0$ for Europium) should fall within the range of 4000 ± 500 cm^{-1} for efficient energy transfer [25]. If the energy gap is less than 1500 cm^{-1}, energy loss due to thermal deactivation may occur [24,25]. Conversely, if the gap is too large, it can adversely affect the efficiency of the energy transfer [24]. Known sensitizers for lanthanide complexes include 2,2′-bipyridines, terpyridines, dipicolinic acid, salicylic acid, benzoate, triphenylenes, substituted phenyl, naphthyl groups, 1,10-phenanthroline, and thenoyltrifluoroacetone [20,24,25]. In this study, thenoyltrifluoroacetone (tta) and bipyridine-based ligands are employed for sensitization. In the initial step of the sensitization, the ligands, acting as an antenna, absorb energy in the UV/visible region and transfer this energy to their triplet state via inter-system crossing (ISC). Subsequently, this energy is transferred to the excited state of the lanthanide(III) metal [23]. In sensing applications, the lanthanide–ligand complex serves as a receptor, with changes in the luminescence properties of the lanthanide(III) metal being induced by the binding analyte [25]. The bound ligand not only shields the lanthanides from solvent quenching but also enhances the analyte binding affinity and contributes to sensitization [25]. The variability in the lifetimes of lanthanide ions, spanning from microseconds (e.g., Yb^{3+}; Nd^{3+}) to milliseconds (e.g., Eu^{3+}; Tb^{3+}), renders them more advantageous for sensor applications [24].

Eu (III) complexes have gained significant prominence as chemosensors in the literature. This heightened interest is primarily attributed to their exceptional qualities as sensors, including high luminous efficiency, long-wavelength emission, and extended lifetimes [14,20]. Additionally, Eu (III) exhibits a ground state ($^7F_0$) and emitting excited state ($^5D_0$) that remains unaffected by crystal-field effects, boasting low J values in the ^7F_J ground state, which greatly simplifies spectrum interpretation [26]. Eu (III) is known for its characteristic line-like emission, which is particularly advantageous for radiometric analysis within the Eu (III) emission spectrum. Typically, in such analyses, the ΔJ = 2 emission at 615 nm and ΔJ = 1 emission at 590 nm are commonly employed [23].

Eu (III) complexes have been effectively employed as chemosensors for the detection of diverse analytes. In 2023, our research group introduced a novel Europium-based complex, $K[Eu(hfa)_4]$, for the detection of dissolved carbon dioxide in an ethylene glycol medium, showcasing its practical utility by enabling real-time monitoring of fermentation reactions [20]. This work leverages the environmental sensitivity of Eu(III) emission and indirectly senses CO_2 via changes in pH in the medium [20]. In 2021, Xu et al. demonstrated the utility of Europium(III)-carbon quantum dots complexes as sensors for mercury (Hg^{2+}) in milk. This complex exhibits dual emissions at 443 and 617 nm, with emission enhancement upon the addition of Hg^{2+} ions [27]. Furthermore, in 2010, Chen et al. synthesized a novel ternary complex based on 2-(2-carboxylphenyl)imidazo[4,5-f]-1,10-phenanthroline-based europium(III) 2-thenoyltrifluoroacetonate. This complex was designed for sensing multiple anions, including F^-, HSO_4^-, and AcO^-. The initial red emission of the sensor changes in response to different anions, owing to hydrogen bonding and competitive coordination with the Eu(III) metal center [28].

Trans-metalation is a thermodynamically driven reaction wherein one organometallic complex transfers its ligands to another metal [29]. Depending on the design, this type of reaction can lead to the generation of two distinct emissions, each associated with the characteristics of the respective metals [30,31]. Alternatively, one metal can act as a quencher, while the other forms the luminescence complex [32]. In the latter method, paramagnetic metals such as Cu^{2+} and Mn^{2+} are frequently employed as quenchers [33–35]. This method finds utility not only in sensing applications but also in organometallic synthesis, catalysis, nanomaterials, metal–organic frameworks, and various other fields [29]. However, the number of reported organometallic complexes serving as chemosensors utilizing transmetalation reactions remains limited [29]. This type of reaction can potentially enhance selectivity due to the shielding function of the newly introduced metal ion [29]. Additionally, the use of different metals with the same ligands may result in distinct thermodynamic

sensing properties [29]. Chemosensors involving Cu/Cd [30], Cu/Cr [32], Cu/Zn [33], Zn/Cd [36], and Zn/Hg [37] replacement reactions have been documented. Most sensing systems based on trans-metalation employ one metal for emission quenching, which is not the most efficient approach for emission enhancement [29]. In our study, we have developed an Eu-based sensor that exhibits two distinct emissions from Eu^{3+} and Al^{3+} complexes, thereby promoting an emission enhancement method.

2. Experimental Section

Materials: The following chemicals are obtained from Sigma Aldrich with the highest available purity and used without further purification: Europium(III) chloride hexahydrate, thenoyltrifluoroacetone, 4,4′-Di-tert-butyl-2,2′-dipyridyl, 1000 mg/L aluminum Standard for ICP in nitric acid, ACS-graded methanol.

Physical measurements: Steady-state photoluminescence (PL) spectra are acquired with a PTI QuantaMaster Model QM-4 scanning spectrofluorometer (HORIBA Instruments Inc., Piscataway, NJ, USA) equipped with a 75-watt xenon arc lamp, the pH measurements are made using a Sper Scientific 840087 Basic pH Meter. Single crystal X-ray diffraction data are obtained on a Rigaku XtaLAB Synergy-S Diffractometer equipped with dual Mo and Cu PhotonJet-S microfocus X-ray sources, a HyPix-6000HE Hybrid Photon Counting detector, and an Oxford Cryostream 800 liquid nitrogen cooling system. Further details about the crystal structure can be found in the Supporting Information. Raman spectra are recorded on a Renishaw InVia system equipped with 785 nm excitation laser, a 1800 L/mm grating and a CCD detector, affording a spectral resolution of 0.2 cm^{-1}. ICP-OES analysis is performed on an iCAP 7000 plus series ICP-OES system (software: QTEGRA).

Synthesis of the [$Eu(tta)_3$([4,4′-$(t\text{-}Bu)_2$]-2,2′-bpy)]: Synthesis of the complex is carried out following a reported procedure [38] with slight modifications. Europium(III) chloride hexahydrate (0.1 g, 0.3 mmol), thenoyltrifluoroacetone (0.198 g, 0.9 mmol), and 4,4′-Di-tert-butyl-2,2′-dipyridyl (0.79 g, 0.1 mmol) are dissolved separately in 5 mL, 2 mL and 2 mL of ethanol, respectively. Then, thenoyltrifluoroacetone solution is added to the Europium (III) chloride hexahydrate solution and mixed well. The pH of the solution is adjusted to 8 by the dropwise addition of triethylamine. After that, the 4,4′-Di-tert-butyl-2,2′-dipyridyl solution is added dropwise to the mixture and stirred at room temperature for one day till a white precipitate forms. The precipitate is filtered and dried under vacuum for 12 h. The yield is 52.5%. Crystals suitable for single-crystal X-ray diffraction experiments are obtained by slow evaporation of the acetone-ethanol solvent. The product is characterized by single-crystal X-ray diffraction (sc-XRD) and ^1H NMR.

Aluminum titration: In all the experiments, the concentration of complex 1 is kept at 1.84×10^{-6} M (0.0496 ppm). The ICP grade 1000 ppm aluminum solution is diluted to 1 ppm with methanol. A volume of 10 µL of the 1 ppm aluminum standard solution is added to 2 mL of complex 1 (1.84×10^{-6} M) solution until saturation. The experiment is repeated three times.

pH studies: An amount of 1 mg of complex 1 is dissolved in methanol to prepare the 1.84×10^{-6} M (0.0496 ppm) solution. Acetic acid and ammonium hydroxide (both at 0.1 M) are used to adjust the pH. The experiments are triplicated.

Selectivity studies: A volume of 50 µL of 0.1 M metal salt solutions is added to 2 mL of 1.84×10^{-6} M (0.0496 ppm) complex 1 solution. Emission spectra are recorded at 398 nm.

Interference studies: The interference study is conducted in two different ways. In the first method, 2 mL of 1.84×10^{-6} M (0.0496 ppm) complex 1 is mixed with 10 µL of 0.1 M metal salt solution, followed by 10 µL of 0.1 M Al^{3+} solution. This procedure is carried out separately for each metal ion. The second approach involved the sequential addition of 10 µL of 0.1 M metal ions to a 2 mL solution of complex 1 in methanol, initially starting with 0.1 M aluminum ions before introducing any other metal ions. The concentration of complex 1 in the solution is 1.84×10^{-6} M (0.0496 ppm).

ICP-OES study: An amount of 5 ppm of aluminum standard solution is prepared using ICP grade 1000 ppm aluminum solution. The prepared 5 ppm solution is used to make the standard and unknown solutions. Finally, 0.2 mL of ICP-graded HNO_3 is added to each solution. A 309.27 nm peak is used for the calibration study. For the parallel PL study, 3 mL of all the prepared solutions are saved before the addition of HNO_3 acid.

Molar ratio method to determine the stoichiometric ratio of Al^{3+} and complex 1: The experiment was performed according to a literature procedure [39–41]. The experiment was started with a fixed volume of complex 1 (1.84×10^{-6} M, 2 mL) and added an increasing volume of 1 ppm of Al^{3+} solution to achieve the different combinations of Al^{3+}/complex 1 molar ratio.

Quantitative detection of Al^{3+} in aluminum-containing water samples as a real-time application. A volume of 10 µL of aluminum-containing water is added to 2 mL of complex 1 (1.84×10^{-6} M) in methanol. After that, the change in luminescence is recorded.

Relative quantum yield measurement: The experiment is performed following the literature procedure [42,43]. A 3.67×10^{-7} M solution of quinine sulfate (QS) is prepared in 0.1 M HCl and the sensor solution is prepared by adding 1 ppm $AlCl_3$ solution to 1×10^{-6} M of Complex 1 solution. Absorption and emission studies are carried out for both standard and sample under similar experimental conditions. The Al^{3+} sensor sample and the quinine sulfate standard are excited at 300 nm for exhibiting comparable absorbance.

3. Results and Discussions

Complex 1 is characterized by single-crystal X-ray diffraction (sc-XRD, Figure 1) and ^{1}H NMR (Figure S1) techniques. The XRD analysis unveils the structure, wherein the Eu (III) center coordinates with six oxygens atoms from three tta (thenoyltrifluoroacetone) ligands and two nitrogen atoms from a ([4,4′-(t-bu)$_2$-2,2′-bpy) ligand, affording an octahedral coordination field for Eu. The average bond lengths for Eu-O and Eu-N are 2.358 Å and 2.577 Å, respectively. It is noteworthy that the specific bond lengths between Eu-O and Eu-N exhibit slight variation within the range of 2.35–2.36 Å and 2.56–2.63 Å, contingent upon the specific ligands employed [44]. These measurements closely align with values documented in the existing literature. Furthermore, the O-Eu-O bond angles displayed deviations from the ideal 90° and 180°, indicative of a subtle geometry distortion from the theoretically perfect octahedral structure (Table S1).

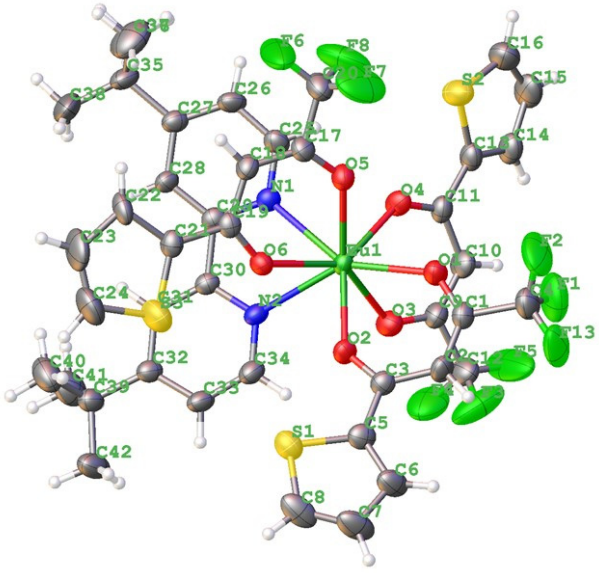

Figure 1. Crystal structure of complex 1. The colours in the structure represent the following atoms: red = oxygen; blue = nitrogen; yellow = sulfur; green = fluorine; grey = carbon; white = hydrogen.

Luminesce properties and trans-metalation

The investigation of the luminescent properties of complex 1 is conducted in methanol at room temperature. The complex exhibits distinct narrow emission bands at 579, 592, 613, and 655 nm, which are assigned to $^5D_0 \rightarrow {}^7F_0$, $^5D_0 \rightarrow {}^7F_1$, $^5D_0 \rightarrow {}^7F_2$, and $^5D_0 \rightarrow {}^7F_3$ transitions of the europium metal center. Notably, the 613 nm emission band displays exceptional intensity and is primarily responsible for the bright red color of the solution. Upon introduction of aluminum ions, trans-metalation is observed, marked by the cessation of europium emission ("turned off") and the onset of aluminum complex emission ("turned on") at 398 nm, as depicted in Figure 2. This transformation resulted in a drastic color change in the solution, which is easily distinguishable under a UV lamp even to the naked eye (inset, Figure 2).

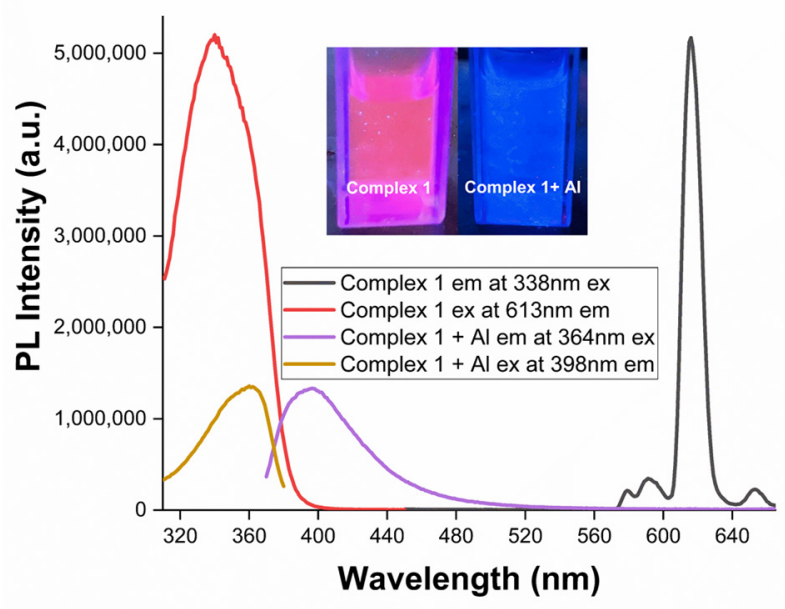

Figure 2. PL spectra of complex 1 in methanol before and after the addition of Al^{3+} ions. (Complex 1: excitation at 338 nm; emission at 613 nm. Complex 1 + Al^{3+}: excitation at 364 nm; emission at 398 nm). The inset picture shows the complex with and without aluminum addition under UV lamp irradiation.

Further experiments are conducted to explore the interaction between Al^{3+} ions and complex 1. The stoichiometry of this interaction is determined using the molar ratio method, keeping the molar amount of complex 1 constant [39–41]. The results conclusively establish a 1:1 ratio between Al^{3+} and complex 1 (Figure 3a). Raman spectroscopy (Figure S2a) reveals the emergence of the Al-O bond vibrations at 418, 495, and 608 cm^{-1} [45] concurrently with the vanishing of the Eu-O and Eu-N bond vibrations at 186, 205, and 215 cm^{-1} [46]. The emergence of new Al-O bonds strongly suggests the coordination of Al^{3+} with the thenoyltrifluoroacetone ligands, while the disappearance of the Eu-O and Eu-N bonds indicates the detachment of the ligands from the europium metal center. This is further corroborated by the absence of the 613 nm peak in the luminescence spectrum (Figure 2). Moreover, the emergence of a new peak at 653 cm^{-1} indicates the formation of Al-N bonds derived from the 4,4′-Di-tert-butyl-2,2′-dipyridyl ligand [47,48] (Figure S2a). Aluminum is known to form six-coordinate complexes with bipyridine-type bidentate ligands [49,50]. With consideration of the Raman data, a possible structure of the aluminum complex is depicted in Figure 3b.

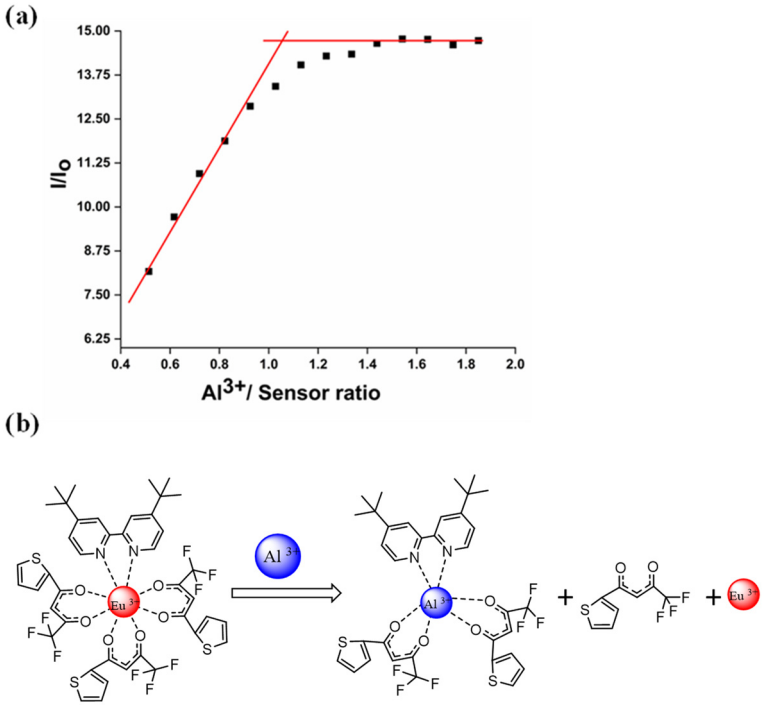

Figure 3. (**a**). Luminescence titration data plot to deduce the 1:1 stoichiometric ratio between Al^{3+} and complex 1. (**b**) Depiction of the binding mode of the Al^{3+} ions (blue circles) by displacing Eu^{3+} ions (red circles) in complex 1.

pH and binding constant studies

The pH investigation aims to assess the sensor's stability across varying pH levels and its applicability in real-world scenarios. The sensor is robust at pH 5–7, particularly promising for bio-related practical uses. Furthermore, it remains stable within the pH range of 5–10, with a noticeable decrease in intensity observed at pH < 5 at 398 nm (Figures 4 and S3).

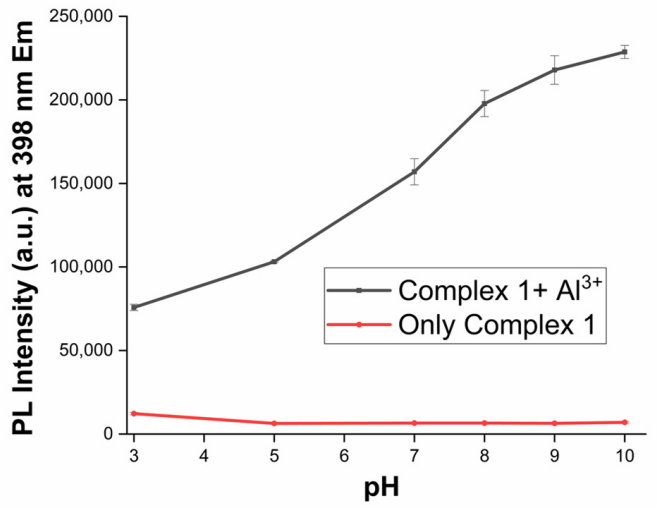

Figure 4. PL response of complex 1 at 398 nm, in the presence and absence of aluminum cation at different pH levels in methanol. (Complex 1: excitation at 338 nm; emission at 613 nm. Complex 1 + Al^{3+}: excitation at 364 nm; emission at 398 nm).

The binding properties of the complex 1 to the aluminum ion are investigated according to the literature. [51,52] The binding constant is obtained from luminescence spectroscopy (see Figure 5) and UV–Vis (Figure S4) methods separately. They are 2.324×10^3

(R^2 = 0.99) and 2.669 × 10^3, respectively (R^2 = 0.99). The average value for the binging constant is 2.496 × 10^3 ± 172. This is consistent with the aluminum binding constants for similar complexes in the literature [21].

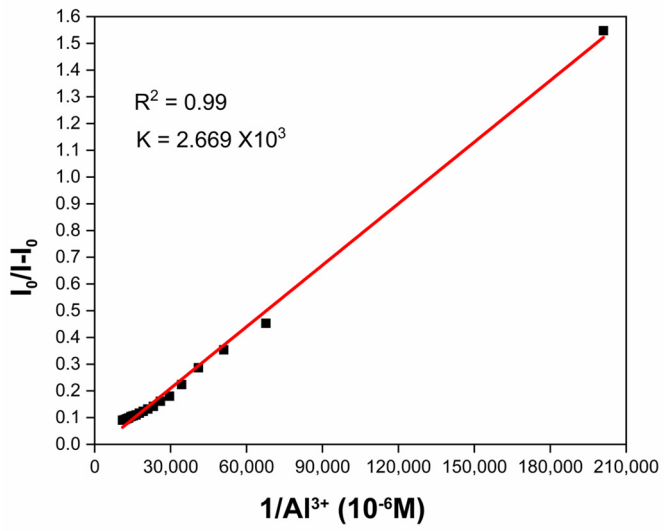

Figure 5. Hildebrand–Benesi plot for PL titration of Al^{3+} into complex 1 in methanol. (Complex 1 + Al^{3+}: excitation at 364 nm; emission at 398 nm).

Sensing of metal ions and selectivity (interference) studies

An exceptional sensor is anticipated to demonstrate superior sensing capabilities and specificity towards the analyte, particularly when compared to various common metals. To evaluate the sensing performance towards common metal ions, an extensive screening involving 12 common metal ions—Zn^{2+}, Cu^{2+}, Co^{2+}, Cd^{2+}, Pb^{2+}, Al^{3+}, Ni^{2+}, Hg^{2+}, K^+, Na^+, Mg^{2+}, and Ca^{2+}—in a methanol solution is conducted (Figures 6a and S5). Remarkably, only the Al^{3+} ion exhibits a distinct peak at 398 nm (above the baseline), while the other metal ions show no luminescence at that wavelength. This notable result emphasizes the sensor's exceptional ability to detect the Al^{3+} ion (Figure 6b).

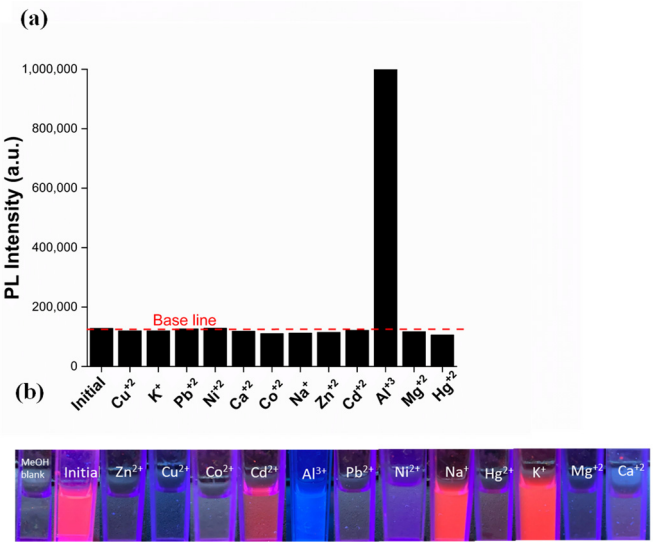

Figure 6. (**a**) PL spectra of complex 1 in methanol upon the addition of Al^{3+} with excitation of 364 nm and emission at 398 nm. (**b**) Photography of complex 1 in the presence of various metal ions under a UV lamp.

The selectivity (interference) study is carried out through two different approaches. In the first method, complex 1 is initially mixed with various other metal ions, followed by the addition of Al^{3+} ions. This procedure is carried out separately for each individual metal ions (Figure 7). In the second method, a scenario is stimulated to mimic a real-life situation in which all metal ions could co-exist in the same medium. In this case, complex 1 and Al^{3+} are mixed first, and subsequently, all the other metal cations are introduced to the same mixture (Figure S8). With both methods, it is clear that the aluminum ion can be detected by the sensor in the presence of most of the s-block and d-block metal ions regardless of single or multiple metal contaminants show casing its high selectivity towards the Al^{3+} ion sensing. It is noteworthy that Cu^{2+}, $Co^{2+,}$ and Cd^{2+} have often been identified as common interferences for aluminum sensors [7,14]. However, our sensor demonstrates no interference with Cu^{2+}, $Co^{2+}$and Cd^{2+} (Figure S8). (See Section 2).

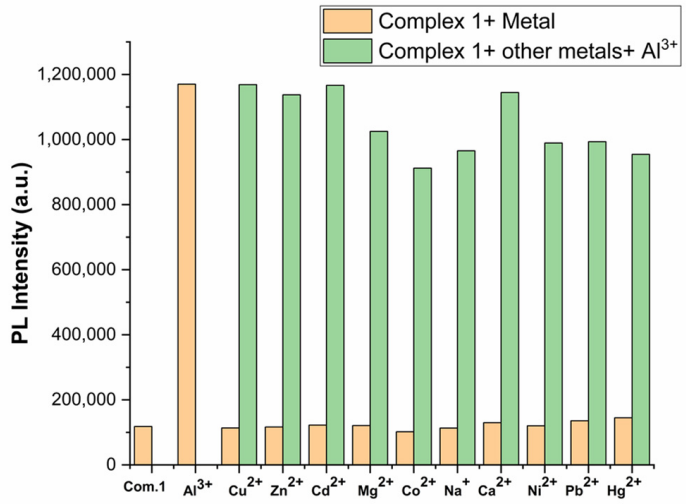

Figure 7. PL responses of complex 1 at 398 nm in the absence and presence of different metal ions in methanol. The first bar (left-most) shows the emission of complex 1 alone; other brown bars represent PL intensities after complex 1 was treated with various metal cations individually, whereas the green bars represent PL intensities after complex 1 was treated with both other metal ions and Al^{3+} simultaneously. A volume of 50 µL of 0.1 M of metal ions was used for all tested metals.

Aluminum titration

Subsequently, an aluminum ion titration is conducted to establish a standard curve. Upon the introduction of Al^{3+} into the sensor solution, a discernible alternation is observed. The peak at 613 nm, responsible for the red emission, decreases in intensity, while a new peak emerges at 398 nm. The notable transformation is harnessed for its ratiometric intensity change, $I_{498}/I_{613,}$ which exhibits a pronounced sensitivity to variations in aluminum concentration, primarily attributed to the hypersensitivity of the J = 2 transition at 613 nm the environment change [14]. Furthermore, the signal-to-noise ratio at 398 nm (I/I_0) demonstrates a remarkable 21-fold increase in signal intensity at saturation, while maintain the linearity within the range of 0–47.6 ppb as evidenced by an R square value of 0.99 (Figures 8 and S6). The limit of detection (LOD) value is 4.79 ppb (1.77×10^{-7} M) calculated as three times the signal-to-noise (I/I_o) ratio. Quantum yield is determined using the quinine sulfate standard by indirect method, the absorbance and emission of QS and Al^{3+} complex are recorded and compared, plugging the values into a standard quantum yield calculator, the aluminum complex is found to exhibit a quantum yield of 0.14, The value is found to be closely related to a known aluminum six coordinated complexes reported in the literature [53]. Refer to Figure S7 for quantum yield data.

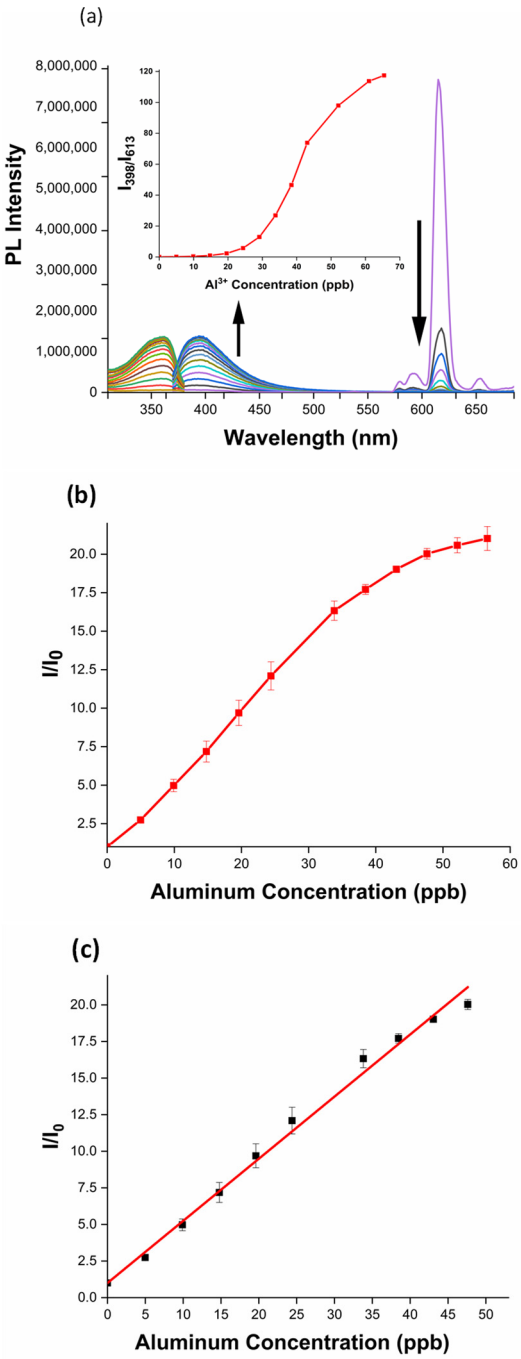

Figure 8. (**a**) PL spectra of complex 1 in methanol upon the addition of Al^{3+} with excitation of 364 nm. The inset presents the standard curve for Al^{3+} addition for I_{398}/I_{613}. (**b**) Standard curve for Al^{3+} addition for I/I_0 at 398 nm emission. (**c**) Linear range for Al^{3+} sensing for complex 1 with an R^2 value = 0.99.

Quantitative detection of Al^{3+} in aluminum-containing water samples as a real-world application.

After thorough investigation of complex 1 for quantitative detection of aluminum ion sensitivity in methanol, endeavors are made to adapt complex 1 for measurements in water samples. A new calibration curve was established for aluminum ions in water (see Section 2). It is essential to underscore that during the calibration procedure, we intentionally introduce 10 µL of water into 2 mL of methanol to ensure the properties of the methanol remain unaffected by the addition of a small quantity of water. This also

accentuates the minimal sample requirement of our sensor for accurate readings. This newly created calibration curve exhibits a linear range of 4.975–24.876 ppb, characterized by a 0.99 R-square value (Figures 9 and S9a,b). The LOD value determined from the graph is 8.11 ppb, set at 3 times the I/I_o value. It is noteworthy to report that this LOD value is much smaller than the WHO-recommended level for aluminum for drinking water. As aluminum serves no discernible function within the human body and its accumulation can result in adverse consequences, our sensor assumes a pivotal role in the detection of even trace amount of aluminum contamination in water. This will help to preservation of water purity and ensure its suitability for consumption. We believe that our sensor holds substantial potential in detecting even trace amount of aluminum ion contaminations, with versatile applications spanning such as monitoring industrial waste water discharge, monitoring water quality in rivers, lakes and oceans, and monitoring public drinking water reservoirs.

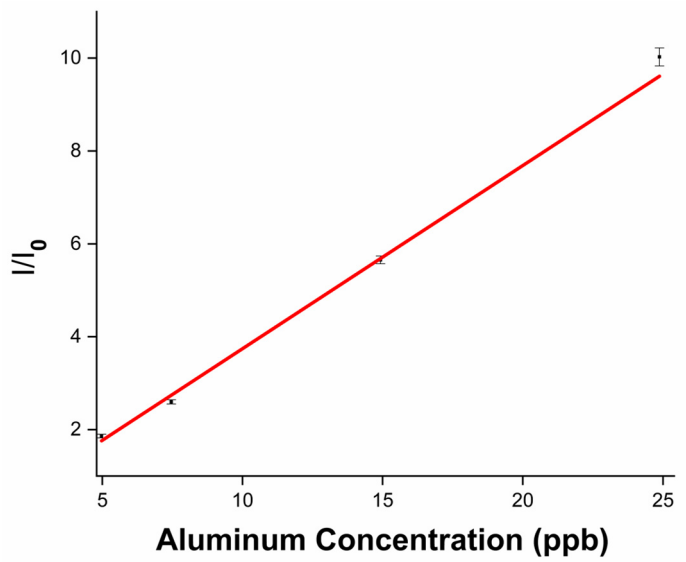

Figure 9. A standard detection curve for Al^{3+} ions by complex 1 in a methanol–water mixture (200:1 *v*/*v*; excitation at 364 nm; emission at 398 nm).

It is worth reporting that the LOD value is smaller, and the range is larger for the aluminum standard curve in methanol than it is in water. The solubility difference of aluminum in methanol and water may be the reason for the difference in LOD and range.

The following equation is derived, where R is the I/I_0 value and Al is the aluminum concentration in ppb:

$$R = 0.39\ [Al] - 0.2$$

To validate the reading of complex 1 for Al^{3+} ions in water, two unknown samples were tested with both the ICP-OES instrument (Figure S10) and complex 1 (Figure S11). Results are summarized in Table 1. The results clearly show the accuracy and repeatability of the readings.

Table 1. A blind study was performed with two unknown samples to validate complex 1's sensing for Al^{3+} ions.

Sample	[Al^{3+}], Calibration Curve (Average of 3 Readings, after Back Calculation)	[Al^{3+}], ICP-OES Readings (Average of 3 Readings)
A	2.051 ppm	2.052 ppm
B	3.779 ppm	3.997 ppm

4. Conclusions

In summary, we have successfully synthesized and characterized a novel highly sensitive, and selective ratiometric optical sensor which can be used in real-life applications. The initial complex, $Eu(tta)_3$ ([4,4′-(t-bu)$_2$-2,2′-bpy)], is characterized by XRD and ^{1}H NMR spectroscopy. The emission at 613 nm gradually disappears upon the addition of aluminum ions and a new peak at 398 nm emerges, demonstrating the ratiometric nature of the sensor. Raman spectroscopy indicates the trans-metalation of the complex upon the addition of aluminum ions to form $Al(tta)_2$([4,4′-(t-bu)$_2$-2,2′-bpy)]. The sensor shows excellent selectivity for Al^{3+} against common s- and d-block metals, including the Cu^{2+}, $Co^{2+,}$ and Cd^{2+} commonly encountered interfering cations. The sensor can quantitatively detect Al^{3+} ions in the range of 0–46.7 ppb with an LOD of 4.79 ppb in methanol. The sensor functions in a broad pH range of 5–10, indicating environmental and biological applicability. The sensor shows promising results with aqueous samples, and it can quantitatively detect Al^{3+} ions in the 4.975–24.876 ppb range with an 8.11 ppb LOD. The sensor readings are validated by ICP-OES.

Supplementary Materials: The following supporting information can be downloaded at: https://www.mdpi.com/article/10.3390/analytica4040031/s1, Table S1: Crystal structure data for the $Eu(tta)_3$([4,4′-(t-bu)$_2$-2,2′-bpy)] complex; Figure S1: ^{1}H NMR spectrum of $Eu(tta)_3$([4,4′-(t-bu)$_2$-2,2′-bpy)] (complex 1); Figure S2: (a) Raman spectra of complex 1 with and without Al^{3+} ions (normalized scattering intensity). (b) The emission spectrum of thenoyltrifluoroacetone (tta) and the Complex1+ Al^{3+}; Figure S3: Effect of pH towards Al^{3+} sensing in methanol (excitation at 364 nm; emission at 398 nm). (a) Trial 01. (b) Trial 02. (c) Trial 03; Figure S4: Determination of binding constant for Al^{3+} sensing in methanol. The Equation used for the calculation is $I_0/(I - I_o) = I_0/(K_a(I - I_o)[Al^{3+}]^{1/2}) + I_0/(I - I_o)$. K_a (binding constant) was solved by Intercept/slop of the graph; Figure S5: Selectivity study of complex 1 for aluminum in methanol (excitation at 364 nm; emission at 398 nm); Figure S6: Linear relationship with Al^{3+} concentration in methanol. Figure S7: Relative quantum yield study (a) Absorption spectra of the Quinine sulfate and the Complex 1 + Al^{3+} solution. (b) Emission spectra of the Quinine sulfate and the Complex 1 + Al^{3+} solution at 301 nm excitation. Figure S8: Interference study with 12 metals in methanol (excitation at 364 nm; emission at 398 nm). Figure S9: (a) Aluminum ion titration in the methanol-water mixture (200:1 v/v). (b) Calibration curve in the methanol-water mixture (200:1 v/v) (excitation at 364 nm; emission at 398 nm). Figure S10: Standard curve for Al^{3+} ions from ICP-OES in Millipore water. Figure S11: Luminescence spectra of Unknown Sample-1 and Unknown Sample-2 in methanol-water mixture (200:1 v/v) (excitation at 364 nm; emission at 398 nm). References [21,54–58] are cited in the supplementary materials.

Author Contributions: Conceptualization, S.B.M. and M.A.O.; methodology, S.B.M. and M.A.O.; formal analysis, N.A.K.R.P., S.K.S., C.M.A., V.N.N. and H.Y.; investigation, N.A.K.R.P.; resources, S.B.M., H.Y. and M.A.O.; data curation, N.A.K.R.P., S.K.S., C.M.A. and V.N.N.; writing—N.A.K.R.P.; writing—review and editing, N.A.K.R.P., S.B.M., H.Y. and M.A.O.; visualization, M.A.O. and S.B.M.; supervision, M.A.O., H.Y. and S.B.M.; project administration, S.B.M. and M.A.O.; funding acquisition, M.A.O. and S.B.M. All authors have read and agreed to the published version of the manuscript.

Funding: This work has been supported by the Welch Foundation (B-1542) and the National Science Foundation (CHE-1413641).

Data Availability Statement: Data is contained within the article or Supplementary Materials.

Acknowledgments: The authors would like to acknowledge Guido F. Verbeck and his group for providing the ICP-OES facility to collect data for the completion of this project. Also, we are grateful to Ph.D. candidate, Murillo Wilbert, for assisting in collecting data on the ICP-OES instrument. Data collected for this paper represent part of the Ph.D. dissertation of Nawagamu A. K. Rajitha Perera.

Conflicts of Interest: The authors declare no conflict of interest.

References

1. Zhou, Y.; Kim, H.; Yoon, J. A selective 'Off-On' fluorescent sensor for Zn^{2+} based on hydrazone-pyrene derivative and its application for imaging of intracellular Zn^{2+}. *Bioorganic Med. Chem. Lett.* **2010**, *20*, 125–128. [CrossRef]

2. Xu, W.; Qi, D.; You, J.; Hu, F.; Bian, J.; Yang, C.; Huang, J. Coumarin-based 'turn-off' fluorescent chemosensor with high selectivity for Cu^{2+} in aqueous solution. *J. Mol. Struct.* **2015**, *1091*, 133–137. [CrossRef]
3. Xu, T.; Duan, H.; Wang, X.; Meng, X.; Bu, J. Fluorescence sensors for Zn^{2+} based on conjugated indole Schiff base. *Spectrochim. Acta Part A Mol. Biomol. Spectrosc.* **2015**, *138*, 603–608. [CrossRef] [PubMed]
4. Xu, H.; Wang, X.; Zhang, C.; Wu, Y.; Liu, Z. Coumarin-hydrazone based high selective fluorescence sensor for copper(II) detection in aqueous solution. *Inorg. Chem. Commun.* **2013**, *34*, 8–11. [CrossRef]
5. Wang, L.; Ye, D.; Cao, D. A novel coumarin Schiff-base as a Ni(II) ion colorimetric sensor. *Spectrochim. Acta Part A Mol. Biomol. Spectrosc.* **2012**, *90*, 40–44. [CrossRef]
6. Gupta, V.K.; Mergu, N.; Kumawat, L.K.; Singh, A.K. A reversible fluorescence "off–on–off" sensor for sequential detection of aluminum and acetate/fluoride ions. *Talanta* **2015**, *144*, 80–89. [CrossRef]
7. Ma, J.; Shi, W.; Feng, L.; Chen, Y.; Fan, K.; Hao, Y.; Hui, Y.; Xie, Z. A highly selective and sensitive acylhydrazone-based turn-on optical sensor for Al^{3+}. *RSC Adv.* **2016**, *6*, 28034–28037. [CrossRef]
8. Goswami, S.; Aich, K.; Das, S.; Das, A.K.; Sarkar, D.; Panja, S.; Mondal, T.K.; Mukhopadhyay, S. A red fluorescence 'off-on' molecular switch for selective detection of Al^{3+}, Fe^{3+} and Cr^{3+}: Experimental and theoretical studies along with living cell imaging. *Chem. Commun.* **2013**, *49*, 10739–10741. [CrossRef]
9. Suryawanshi, V.D.; Gore, A.H.; Dongare, P.R.; Anbhule, P.V.; Patil, S.R.; Kolekar, G.B. A novel pyrimidine derivative as a fluorescent chemosensor for highly selective detection of Aluminum (III) in aqueous media. *Spectrochim. Acta Part A Mol. Biomol. Spectrosc.* **2013**, *114*, 681–686. [CrossRef]
10. Shinde, S.; Kim, D.; Saratale, R.G.; Syed, A.; Ameen, F.; Ghodake, G. A Spectral Probe for Detection of Aluminum (III) Ions Using Surface Functionalized Gold Nanoparticles. *Nanomaterials* **2017**, *7*, 287. [CrossRef]
11. Huang, M.; Lai, J.; Sun, H.; Wu, W. A simple, highly selective and ultra-sensitive "off-on-off" fluorescent chemosensor for successive detection of aluminum ion and phosphate in water samples. *Microchem. J.* **2019**, *151*, 104195. [CrossRef]
12. Liu, Y.; Bi, A.; Gao, T.; Cao, X.; Gao, F.; Rong, P.; Wang, W.; Zeng, W. A novel self-assembled nanoprobe for the detection of aluminum ions in real water samples and living cells. *Talanta* **2019**, *194*, 38–45. [CrossRef] [PubMed]
13. Peng, H.; Han, Y.; Lin, N.; Liu, H. Two pyridine-derived Schiff-bases as turn-on fluorescent sensor for detection of aluminium ion. *Opt. Mater.* **2019**, *95*, 109210. [CrossRef]
14. Xu, W.; Zhou, Y.; Huang, D.; Su, M.; Wang, K.; Hong, M. A Highly Sensitive and Selective Fluorescent Sensor for Detection of Al^{3+} Using a Europium(III) Quinolinecarboxylate. *Inorg. Chem.* **2014**, *53*, 6497–6499. [CrossRef]
15. Fu, Y.; Jiang, X.; Zhu, Y.; Zhou, B.; Zang, S.; Tang, M.; Zhang, H.; Mak, T.C.W. A new fluorescent probe for Al^{3+} based on rhodamine 6G and its application to bioimaging. *Dalton Trans.* **2014**, *43*, 12624. [CrossRef]
16. Polle, E.; Konzak, C.F.; Kattrick, J.A. Visual Detection of Aluminum Tolerance Levels in Wheat by Hematoxylin Staining of Seedling Roots. *Crop Sci.* **1978**, *18*, 823–827. [CrossRef]
17. Martin, J.W.; Stark, T.D.; Thalhamer, T.; Gerbasi-Graf, G.T.; Gortner, R.E. Detection of Aluminum Waste Reactions and Waste Fires. *J. Hazard. Toxic Radioact. Waste* **2013**, *17*, 164–174. [CrossRef]
18. Park, H.; Kim, W.; Kim, M.; Lee, G.; Lee, W.; Park, J. Eco-friendly and enhanced colorimetric detection of aluminum ions using pectin-rich apple extract-based gold nanoparticles. *Spectrochim. Acta Part A Mol. Biomol. Spectrosc.* **2021**, *245*, 118880. [CrossRef]
19. Mohan, N.; Sreejith, S.S.; Begum, P.M.S.; Kurup, M.R.P. A modern approach for the sensing of aqueous Al(III) ion by Ni(II) Salen-type Schiff base complexes. *Appl. Organomet. Chem.* **2019**, *33*, e5064. [CrossRef]
20. Benton, E.N.; Perera, N.A.K.R.; Nesterov, V.N.; Perera, W.; Omary, M.A.; Marpu, S.B. A europium-based optical sensor for the detection of carbon dioxide and its application for a fermentation reaction. *Chemosensors* **2023**, *11*, 5. [CrossRef]
21. Song, H.; Liu, G.; Fan, C.; Pu, S. A novel fluorescent sensor for Al^{3+} and Zn^{2+} based on a new europium complex with a 1,10-phenanthroline ligand. *J. Rare Earths* **2021**, *39*, 460–468. [CrossRef]
22. Weitz, E.A.; Pierre, V.C. A ratiometric probe for the selective time-gated luminescence detection of potassium in water. *Chem. Commun.* **2011**, *47*, 541–543. [CrossRef]
23. Bodman, S.E.; Butler, S.J. Advances in anion binding and sensing using luminescent lanthanide complexes. *Chem. Sci.* **2021**, *12*, 2716–2734. [CrossRef]
24. Parker, D. Luminescent lanthanide sensors for pH, pO_2 and selected anions. *Coord. Chem. Rev.* **2000**, *205*, 109. [CrossRef]
25. Cable, M.L.; Levine, D.J.; Kirby, J.P.; Gray, H.B.; Ponce, A. Luminescent lanthanide sensors. *Inorg. Photochem.* **2011**, *63*, 1.
26. Binnemans, K. Interpretation of europium(III) spectra. *Coord. Chem. Rev.* **2015**, *295*, 1–45. [CrossRef]
27. Gan, Z.; Hu, X.; Huang, X.; Li, Z.; Zou, X.; Shi, J.; Zhang, W.; Li, Y.; Xu, Y. A dual-emission fluorescence sensor for ultrasensitive sensing mercury in milk based on carbon quantum dots modified with europium (III) complexes. *Sens. Actuators B Chem.* **2021**, *328*, 128997. [CrossRef]
28. Wang, Q.; Tan, C.; Tamiaki, H.; Chen, H. Emission response towards three anions (F−, HSO4− and AcO−) by a luminescent europium ternary complex with a 2-arylimidazole-1,10-phenanthroline conjugate. *Photochem. Photobiol. Sci.* **2010**, *9*, 791–795. [CrossRef] [PubMed]
29. Cheng, J.; Ma, X.; Zhang, Y.; Liu, J.; Zhou, X.; Xiang, H. Optical Chemosensors Based on Transmetalation of Salen-Based Schiff Base Complexes. *Inorg. Chem.* **2014**, *53*, 3210–3219. [CrossRef] [PubMed]
30. Royzen, M.; Dai, Z.; Canary, J.W. Ratiometric Displacement Approach to Cu(II) Sensing by Fluorescence. *J. Am. Chem. Soc.* **2005**, *127*, 1612–1613. [CrossRef] [PubMed]

31. Maity, D.; Govindaraju, T. A differentially selective sensor with fluorescence turn-on response to Zn^{2+} and dual-mode ratiometric response to Al^{3+} in aqueous media. *Chem. Commun.* **2012**, *48*, 259–261. [CrossRef]
32. Wang, J.; Qi, Q.; Zhang, L.; Li, S. Turn-On Luminescent Sensing of Metal Cations via Quencher Displacement: Rational Design of a Highly Selective Chemosensor for Chromium(III). *Inorg. Chem.* **2012**, *51*, 1325–1329. [CrossRef] [PubMed]
33. Khatua, S.; Choi, S.H.; Lee, J.; Huh, J.O.; Do, Y.; Churchill, D.G. Highly Selective Fluorescence Detection of Cu^{2+} in Water by Chiral Dimeric Zn^{2+} Complexes through Direct Displacement. *Inorg. Chem.* **2009**, *48*, 1799–1801. [CrossRef]
34. You, Y.; Tomat, E.; Hwang, K.; Atanasijevic, T.; Nam, W.; Jasanoff, A.P.; Lippard, S.J. Manganese displacement from Zinpyr-1 allows zinc detection by fluorescence microscopy and magnetic resonance imaging. *Chem. Commun.* **2010**, *46*, 4139–4141. [CrossRef] [PubMed]
35. He, G.; Zhao, Y.; He, C.; Liu, Y.; Duan, C. "Turn-On" Fluorescent Sensor for Hg^{2+} via Displacement Approach. *Inorg. Chem.* **2008**, *47*, 5169–5176. [CrossRef]
36. Xue, L.; Liu, Q.; Jiang, H. Ratiometric Zn^{2+} fluorescent sensor and new approach for sensing Cd^{2+} by ratiometric displacement. *Org. Lett.* **2009**, *11*, 3454–3457. [CrossRef]
37. Lee, J.W.; Jung, H.S.; Kwon, P.S.; Kim, J.W.; Bartsch, R.A.; Kim, Y.; Kim, S.; Kim, J.S. Chromofluorescent Indicator for Intracellular Zn^{2+}/Hg^{2+} Dynamic Exchange. *Org. Lett.* **2008**, *10*, 3801–3804. [CrossRef] [PubMed]
38. De Silva, C.R.; Maeyer, J.R.; Wang, R.; Nichol, G.S.; Zheng, Z. Adducts of europium β-diketonates with nitrogen p, p′-disubstituted bipyridine and phenanthroline ligands: Synthesis, structural characterization, and luminescence studies. *Inorg. Chim. Acta* **2007**, *360*, 3543–3552. [CrossRef]
39. Sakur, A.A.; Chalati, T.; Fael, H. Selective spectrofluorimetric method for the determination of perindopril erbumine in bulk and tablets through derivatization with dansyl chloride. *J. Anal. Sci. Technol.* **2015**, *6*, 1–12. [CrossRef]
40. El-Didamony, A.M.; Saad, M.Z.; Ramadan, G.M. Charge-transfer complexes of chlorphenoxamine hydrochloride with chloranilic acid, 2,3-dichloro-5,6-dicyano-1,4-benzoquinone and 7,7,8,8-tetracyanoquinodimethane as π-acceptors. *Int. J. Appl. Pharm.* **2019**, *11*, 117–123. [CrossRef]
41. Jumean, F.; El-Dakiky, M.; Manassra, A.; Kareem, M.A.; Alhaj, M.A.; Khamis, M. Complexing Properties of Acid Alizarin Violet with Copper, Cobalt and Nickel in Micellar Media Containing SDS, CTAB and TX-100. *Am. J. Anal. Chem.* **2014**, *5*, 1–7. [CrossRef]
42. Hu, J.; Zhang, C. Simple and Accurate Quantification of Quantum Yield at the Single-Molecule/Particle Level. *Anal. Chem.* **2013**, *85*, 2000–2004. [CrossRef]
43. Nagaraja, D.; Melavanki, R.M.; Patil, N.R.; Geethanjali, H.S.; Kusanur, R.A. Solvent effect on the relative quantum yield and fluorescence quenching of a newly synthesized coumarin derivative. *Luminescence* **2015**, *30*, 495–502. [CrossRef] [PubMed]
44. Tsaryuk, V.I.; Zhuravlev, K.P.; Szostak, R.; Vologzhanina, A.V. Structure, luminescence, and Raman spectroscopy of europium and terbium dipivaloylmethanates and other β-diketonates with 2,2′-bipyridine. *J. Struct. Chem.* **2020**, *61*, 1026–1037. [CrossRef]
45. Misra, A.; Bist, H.D.; Navati, M.S.; Thareja, R.K.; Narayan, J. Thin film of aluminum oxide through pulsed laser deposition: A micro-Raman study. *Mater. Sci. Eng. B* **2001**, *79*, 49. [CrossRef]
46. Tsaryuk, V.; Zolin, V.; Legendziewicz, J.; Szostak, R.; Sokolnicki, J. Effect of ligand radicals on vibrational IR, Raman and vibronic spectra of europium β-diketonates. *Spectrochim. Acta. Part A Mol. Biomol. Spectrosc.* **2005**, *61*, 185–191. [CrossRef] [PubMed]
47. Cao, Y.G.; Chen, X.L.; Lan, Y.C.; Li, J.Y.; Xu, Y.P.; Xu, T.P.; Liu, Q.L.; Liang, J.K. Blue emission and Raman scattering spectrum from AlN nanocrystalline powders. *J. Cryst. Growth* **2000**, *213*, 198. [CrossRef]
48. Liu, L.; Liu, B.; Edgar, J.H.; Rajasingam, S.; Kuball, M. Raman characterization and stress analysis of AlN grown on SiC by sublimation. *J. Appl. Phys.* **2002**, *92*, 5183–5188. [CrossRef]
49. Decarlo, S.; Mayo, D.H.; Tomlinson, W.; Hu, J.; Hooper, J.; Zavalij, P.; Bowen, K.; Schnöckel, H.; Eichhorn, B. Synthesis, Structure, and Properties of $Al(Rbpy)_3$ Complexes (R = t-Bu, Me): Homoleptic Main-Group Tris-bipyridyl Compounds. *Inorg. Chem.* **2016**, *55*, 4344. [CrossRef]
50. Ng, S.M.; Narayanaswamy, R. Fluorescence sensor using a molecularly imprinted polymer as a recognition receptor for the detection of aluminium ions in aqueous media. *Anal. Bioanal. Chem.* **2006**, *386*, 1235–1244. [CrossRef]
51. Hill, J.P.; El-Khouly, M.E.; Charvet, R.; Subbaiyan, N.K.; Ariga, K.; Fukuzumi, S.; D'Souza, F. Effect of anion binding on charge stabilization in a bis-fullerene–oxoporphyrinogen conjugate. *Chem. Commun.* **2010**, *46*, 7933–7935. [CrossRef] [PubMed]
52. Hill, J.P.; Schumacher, A.L.; D'Souza, F.; Labuta, J.; Redshaw, C.; Elsegood, M.R.J.; Aoyagi, M.; Nakanishi, T.; Ariga, K. Chromogenic Indicator for Anion Reporting Based on an N-Substituted Oxoporphyrinogen. *Inorg. Chem.* **2006**, *45*, 8288–8296. [CrossRef] [PubMed]
53. Pérez-Bolívar, C.; Takizawa, S.; Nishimura, G.; Montes, V.A.; Anzenbacher, P., Jr. High-Efficiency Tris(8-hydroxyquinoline)aluminum (Alq_3) Complexes for Organic White-Light-Emitting Diodes and Solid-State Lighting. *Chem. Eur. J.* **2011**, *17*, 9076–9082. [CrossRef] [PubMed]
54. Sheldrick, G.M. *SHELXT*—Integrated space-group and crystal-structure determination. *Acta Cryst.* **2015**, *A71*, 3–8. [CrossRef] [PubMed]
55. Sheldrick, G.M. Crystal structure refinement with *SHELXL*. *Acta Cryst.* **2015**, *C71*, 3–8.
56. Spek, A.L. Structure validation in chemical crystallography. *Acta Cryst.* **2009**, *D65*, 148–155. [CrossRef] [PubMed]

57. Dolomanov, O.V.; Bourhis, L.J.; Gildea, R.J.; Howard, J.A.K.; Puschmann, H. *OLEX2*: A complete structure solution, refinement and analysis program. *J. Appl. Cryst.* **2009**, *42*, 339–341. [CrossRef]
58. Yadav, P.; Gond, S.; Singh, A.; Singh, V.P. Development of a reversible chromogenic sensor for Cu^{2+} in aqueous ethanol. *Mater. Lett.* **2021**, *295*, 129869. [CrossRef]